Nanoscale Advances

Accepted Manuscript

This article can be cited before page numbers have been issued, to do this please use: H. B. Rathod, A. Deshmukh, Y. Desai and P. N. Patel, *Nanoscale Adv.*, 2026, DOI: 10.1039/D6NA00174B.

ROYAL SOCIETY OF CHEMISTRY

rsc.li/nanoscale-advances

ARTICLE Nanoscale Advances

Palladium Bio-Nanocomposite as an Efficient Heterogeneous Catalyst for Nitro Reduction: Fungus Mediated Green and Sustainable Process

View Article Online
DOI: 10.1039/D6NA00174B

Hemal B. Rathod, Amar G. Deshmukh, Yashasvi N. Desai, Paresh N. Patel*

Received 00th January 20xx,
Accepted 00th January 20xx

DOI: 10.1039/x0xx00000x

Abstract: Metallic nanocatalysts such as Palladium nanoparticles (Pd-NPs) possess remarkable catalytic activity owing to their high surface-to-volume ratio; however, aggregation and metal leaching significantly compromise their stability and practical applicability. In this work, we report a facile and sustainable biosynthetic route for the preparation of bio-stabilized Pd-NPs using the fungal strain *Aspergillus trinidadensis* VM ST01 (OL587588) as a green reducing and capping agent. The strategy enables simultaneous bio-reduction of Pd^{2+} ions, nucleation and *in-situ* surface functionalization without the use of hazardous chemicals, surfactants, buffer, or external stabilizers. The influence of culture age (24–54 h), biomass loading (0.08–0.24 g/mL), and incubation time (8–24 h) on NPs formation was systematically investigated to achieve controlled synthesis. Comprehensive physicochemical characterization (UV–Vis, FT-IR, XRD, SEM, TEM, elemental mapping, EDX, XPS, and TGA) confirmed the formation of uniformly distributed Pd-NPs with an average size of ~35 nm, embedded and stabilized within the fungal biomass matrix. The bio-organic framework surrounding the nanoparticles effectively suppresses aggregation and minimizes palladium leaching, thereby enhancing catalyst durability. The catalytic performance of the biosynthesized AtPdNPs was evaluated for the hydrogenation of nitro-benzene (NB) to amino-benzene (AB) as a model reaction under mild and aqueous conditions ($NaBH_4$, ambient temperature and pressure). The optimized catalyst (0.16 g/mL biomass, 36 h culture age, 24 h incubation) achieved complete conversion within 30 min, delivering a turnover frequency (TOF) of 832 h^{-1} and a turnover number (TON) of 416. The kinetics for the reduction of NB to AB was investigated and the catalytic activity of AtPdNPs was evaluated with pseudo first-order rate constant (k_{app}). The *in-situ* bio-coating of AtPdNPs significantly reduces palladium leaching (< 1.5% ppm), enhances storage stability and make it environmentally compatible material. As a result, catalyst maintains its structural integrity and catalytic performance under industry relevant conditions.

1. Introduction

Materials incorporating Palladium play a dynamic role in diverse research areas, including water purification,[1,2] electrochemistry,[3,4] drug delivery,[5] sensing,[6] and organic transformations.[7-9] In particular, palladium nanoparticles (Pd-NPs) have attracted significant attention owing to their enhanced physicochemical and optical properties at the nanoscale.[10–12] The high surface-to-volume ratio and abundant active sites of Pd-NPs make them highly efficient catalysts, especially in reduction reactions and carbon–carbon coupling processes.[13–16] Beyond synthetic chemistry, Pd-NPs are widely applied in environmental remediation for pollutant degradation and exhaust gas treatment.[17] Their antimicrobial activity, arising from reactive oxygen species (ROS) generation and membrane disruption, has also enabled applications in medical devices, drug delivery systems, diagnostics, and photo thermal cancer therapy (**Figure 1**).[18,19]

Conventionally, Pd-NPs are synthesized *via* chemical reduction,[20] electrochemical deposition,[21] and thermal decomposition methods.[22,23] Although these approaches can produce high-quality nanoparticles, they frequently require toxic reducing agents, stabilizers, or organic ligands. Such processes may generate hazardous by-products, limit large-scale sustainability, and leave residual surface contaminants that adversely affect catalytic and biological performance.[24] Moreover, nanoparticle aggregation remains a persistent challenge, leading to diminished catalytic efficiency and stability.[25] Currently, the growing interest in sustainable and environmentally friendly processes has led to the development of green synthetic methods for PdNPs.[26] (**Figure 1**)

In response to increasing environmental concerns, green and sustainable synthetic methodologies for Pd-NPs have gained considerable attention.[27,28] Several publications in literature describe the production of metal nanoparticles (NPs) using different biomaterials which emphasize the safe, non-toxic and ecologically friendly character.[29–33] The integration of nanotechnology and biotechnology, often termed nanobiotechnology, offers innovative pathways for environmentally benign nanomaterial fabrication.[34–36] Biogenic synthesis using plant extracts, bacteria, or fungi provides a promising alternative to conventional

Laboratory of Bio-Organic Chemistry, Tarsadia Institute of Chemical Science (TICS), Uka Tarsadia University, Bardoli – 394 350, Gujarat, India.
pareshn111@yahoo.com

† Footnotes relating to the title and/or authors should appear here.
Supplementary Information available: [details of any supplementary information available should be included here]. See DOI: 10.1039/x0xx00000x

physicochemical routes.[37,38] These biological systems contain naturally occurring biomolecules capable of acting simultaneously as reducing and stabilizing agents, enabling nanoparticles formation under mild conditions without need for external toxic chemicals.[39-41] Importantly, *in-situ* bio-functionalization can minimize aggregation and eliminate the necessity for additional capping agents. Strictly "green" methods can be used to synthesize nanoparticles by using environmentally friendly solvent systems and safe reducing and stabilizing agents.[42,43] Green synthesis of Pd-NPs uses natural reducing agents like plant extracts, bacteria, or fungi to reduce palladium salts, making it environmentally friendly, biocompatible, and producing unique properties. These methods are cost-effective, sustainable, and reduces environmental impact.[44] Plant extracts contain bioactive compounds that act as reducing and capping agents, resulting in stable, uniformly dispersed nanoparticles. Microbial synthesis using bacteria and fungi offers an eco-friendly alternative, producing distinct morphological and functional nanoparticles under mild conditions.[45] Nevertheless, impact of an additional capping agent or stabilizer can easily be avoided due to *in-situ* stabilization of the catalyst by the bio-molecules tethered to the metal centre.[46-47] Fungal systems are particularly attractive due to their high metal tolerance, rich enzymatic machinery, and abundant extracellular proteins that facilitate controlled nanoparticles formation and stabilization.[27,38]

Inspired by these advantages and in continuation of our efforts toward sustainable nanoparticles development,[27,37] we herein report a green biosynthetic strategy for the preparation of bio-stabilized Pd-NPs. The synthesized catalyst demonstrates excellent performance in the reduction of nitrobenzene to aniline under environmentally benign conditions, delivering high turnover frequency (TOF) and turnover number (TON). This study highlights a sustainable and biologically integrated approach for designing efficient Pd-based heterogeneous nano catalysts.

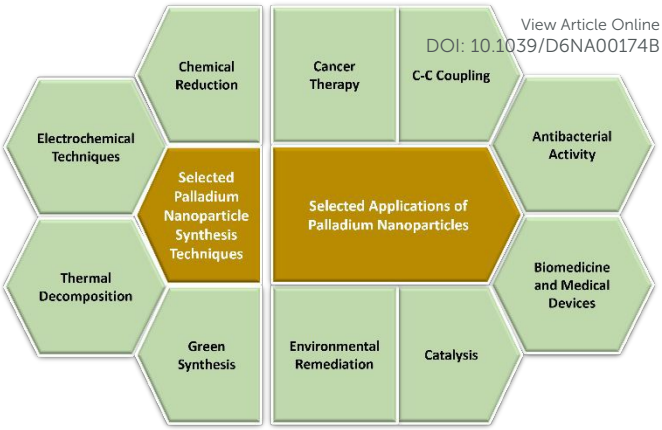

Figure 1. Selected techniques for synthesis and applications of Palladium nanoparticle

2. Experiment

2.1 Chemicals and Characterization Techniques:

Palladium (II) chloride (Reagent Plus®, 99%) is purchased from Sigma-Aldrich. Nitrobenzene, Aniline, Acetonitrile (HPLC), and H_2O (HPLC) are purchased from Rankem. Potato Dextrose Broth (Granulated) and Potato Dextrose Agar are purchased from Hi-Media. Laboratory-prepared double-distilled water.

UV-Vis Spectroscopy (Shimadzu UV-1900i), Zeta size and zeta potential (Malvern Zetasizer Lab), Fourier Transform Infrared Spectroscopy (FT-IR) (Bruker FT-IR ALPHA II), Powder X-ray diffraction (PXRD) (Malvern Panlytical X`pert Pro), Energy Dispersive X-ray Spectroscopy (EDX), and X-ray Photoelectron Spectroscopy (XPS) (Shimadzu Axis Supra Kratis Ultra-II system), Scanning Electron Microscopy (SEM), Transmission Electron Microscopy (TEM), Thermogravimetric Analysis (TGA) and Differential Scanning Calorimetry (DSC) (Mettler Toledo), High Performance Liquid Chromatography (HPLC) (Shimadzu Prominence-i LC 2030 Plus).

2.2 Isolation and Growth of Aspergillus trinidadensis VM ST01' OL587588 (At) (Fungi):

The *Aspergillus trinidadensis* VM ST01' OL587588 (At) (Fungi) was selected for this study. It was extracted from the soil of our campus garden and established with the support of our Microbiology

View Article Online
DOI: 10.1039/D6NA00174B

Department. Optics microscopy and lactophenol cotton blue staining were used to examine the strain's morphology. This fungal strain's pure culture was maintained on Potato Dextrose Agar slants.[27]

Potato dextrose agar (39.0 gm) was dissolved in a one liter of distilled water. Resultant solution was heated at its boiling point to completely dissolve the media. Later on it was sterilize using an autoclave set to the validated cycle, or for 15 minutes at 121 °C and 15 kg/cm^2 of pressure. Then reduce the temperature to between 40 and 45 °C. After blending well, transferred to sterilized Petri dishes and incubate at 36 °C for 72 h. Every month, the slants were prepared and maintained.

After this the primary media was prepared by dissolving 24 gm of potato dextrose broth in one Lit of distilled water. To completely dissolve the medium necessary was applied. Then it was sterilize by autoclave at 15 kg/cm^2 of pressure and 121 °C for 15 minutes. After that the culture from the agar slant was charged at room temperature, about 25 °C, and incubated for different time intervals at 32 °C and 150 RPM. The resultant bio-mass was separated by using a centrifuge set at 3000 RPM for 5 minutes and media was removed from the biomass. It was washed with sterile double-distilled water, repeat the entire process of centrifugation three times and biomass (fungi) was collected.

2.3 Palladium nanoparticles (AtPdNP) synthesis using Aspergillus trinidadensis (At):

A 1 M stock solution of Palladium (II) Chloride ($PdCl_2$) in 100 mL sterile distilled water (a metal precursor) was prepared. Secondly, a wet biomass (4 gm of 48 h age culture) was re-suspend the into the 25 mL metal solution with a concentration of 1 mM. The obtained solution was incubated for 24 h at 32 °C and 150 RPM. The resulted bio-nano-composite (AtPdNP) was centrifuged for five minutes at 3000 RPM and 25 °C. The process of centrifugation was repeated for washing with distilled water. Finally the palladium nanoparticles doped with biomass (AtPdNP) was dried using a lyophilizer (**Figure 2**). A reference sample devoid of biomass and an additional sample devoid of metal solution are also conducted in the same condition as a controlled experiment.

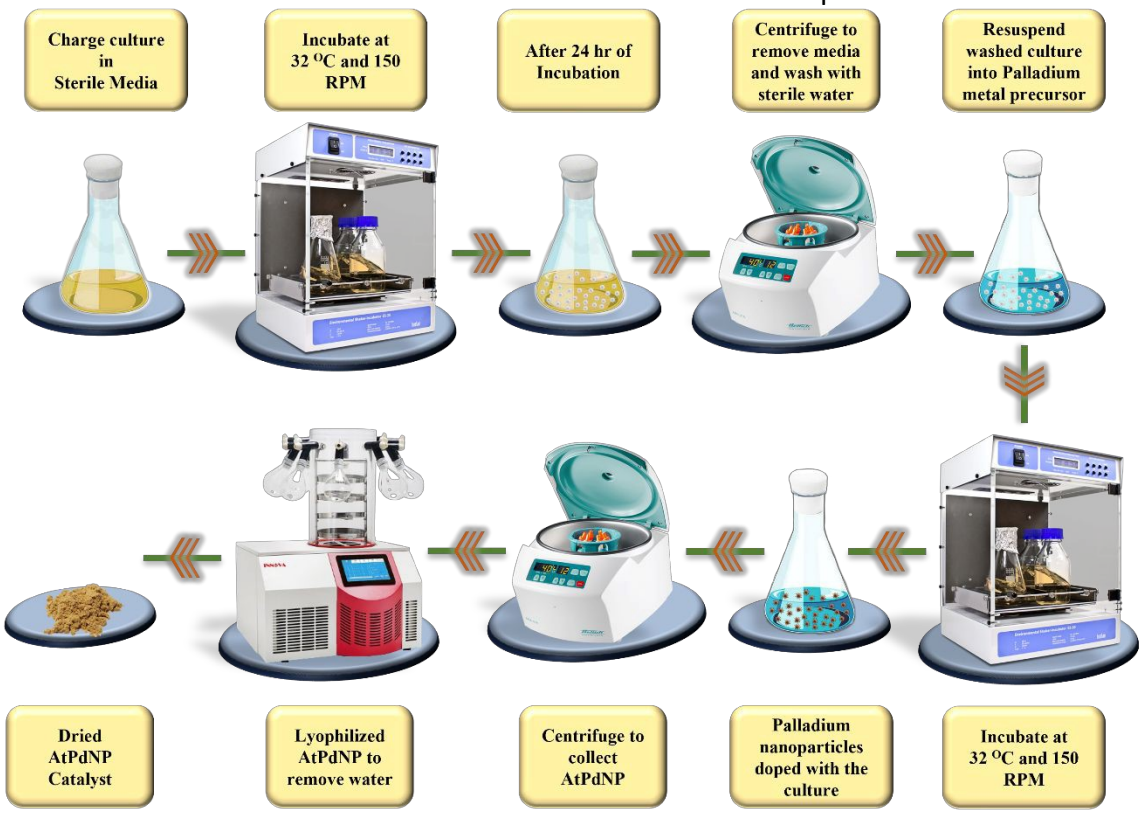

Figure 2: Graphical representation of procedure for AtPdNP synthesis

View Article Online
DOI: 10.1039/D6NA00174B

As an optimisation process, several cultures age (24, 30, 40, 48, and 55 h) were used with fixed biomass concentration (160 mg/mL), metal concentration (1 mM) and 24 h of incubation for AtPdNP synthesis. UV-Vis Spectroscopy and the catalytic activity of prepared AtPdNP were used to determine the optimal culture age for the process. As a second optimization, various biomass concentrations (80 mg/mL, 120 mg/mL, 160 mg/mL, 200 mg/mL, and 240 mg/mL) were used with a 24 h culture age, 1 mM metal concentration and 24 h of incubation. Here also, UV-Vis Spectroscopy and the catalytic activity of prepared AtPdNP were used to determine the optimal biomass content. The production of palladium nanoparticles were further optimised by varying the incubation time (8, 16, or 24 h) with fixed other parameters, i.e. 24 h age culture, 120 mg/mL biomass and 1 mM metal solution concentration. UV-Vis Spectroscopy and the catalytic activity of AtPdNP are used to determine the optimal incubation time for synthesis.

2.4 Process development for nitro reduction with AtPdNP:

Application of prepared AtPdNP was demonstrated for catalytic hydrogenation. As a modal example, process for hydrogenation of nitrobenzene was developed. Dried catalyst AtPdNP (5 mg) was re-suspended in 5 mL of double-distilled water and 1 mM (0.102 mL) of nitrobenzene was added in to 25 mL of RBF. The RBF was then placed in an ice bath and kept at a temperature between 0 and 5 °C. Afterword, 0.075 gm (2 mM) of $NaBH_4$ was added as a hydride source and the reaction flask was tightly sealed to prevent gas leaking. After 5 min the ice bath was removed and resultant solution was stirred at room temperature. Thin-layer chromatography and ninhydrin staining were used to monitor the reaction. Once the reduction was finished, 5 mL of ethyl acetate was added and mixed thoroughly. Then it was allowed to settle in stable conditions to extract the product and separate the layers. After separating the organic phase and drying it by sodium sulphate anhydrous, ethyl acetate was evaporated to collect the final product. (**Scheme 1**) Residual catalyst was washed properly with water and reused for second batch.

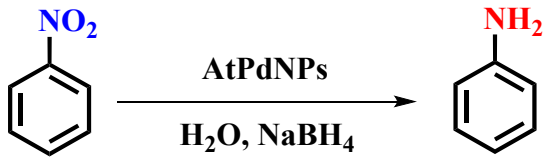

Scheme 1. Reduction of Nitrobenzene using AtPdNP

2.5 Kinetic study for nitro reduction with AtPdNP:

To perform the kinetic study, a conversion of nitro-benzene (NB) to amino-benzene (AB) was quantitatively analysed using spectrophotometry. Initially a maxim um absorption (λmax) was recorded at 260 nm for NB and after completion of reaction it was gradually shifted to 235 nm for AB. The absorption peak at 260 nm decreases with time, indicating the reduction of NB (**Figure 3**).

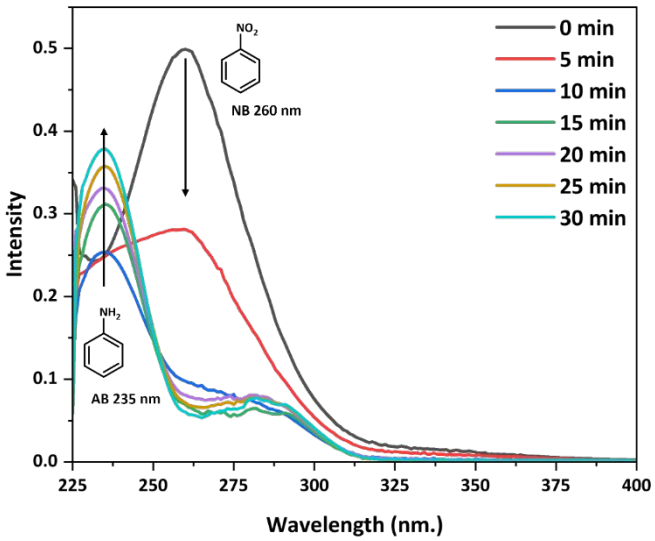

Figure 3: NB to AB reaction study by UV-Vis

The pseudo first-order rate constants (k_{app}) were calculated by fitting the first-order rate constant equation for $\ln(A_0/A_t)$ values against t(s) with a linear fit, where, A_0 and A_t are the initial

View Article Online
DOI: 10.1039/D6NA00174B

absorbance and absorbance after a given time, respectively. The correlation coefficients, *i.e.*, *r* values for this linear fits, varied from 0.96 to 0.99. The k_{app} values were obtained with an accuracy of ±5%. The experimental k_{app} values are the average values for triplicate experiments at temperature 298.15 K (**Figure 4**).

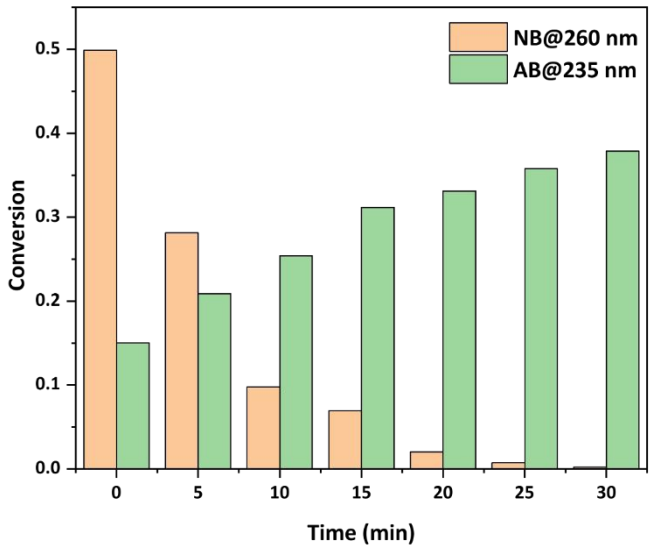

Figure 4: Conversion of NB to AB based on UV-Vis absorbance

2.6 Studies on pH, storage stability and catalyst leaching:

To perform the pH stability of catalyst AtPdNP, aqueous solution with different pH were prepared. A double distilled water was utilised as the primary medium; HCL was employed for its acidic nature, while NaOH was utilised for its basic nature. After making pH solutions ranging from 2, 4, 6, 8, 10 and 12, catalyst AtPdNP was re-suspend into the different pH solutions and let them sit for a day. After 24 h, its efficiency was evaluated by catalytic activity and UV-Vis to make sure there hasn't been any noticeable change. To perform the storage stability of catalyst AtPdNP, the catalyst sample was stored for six months at ambient conditions. The AtPdNP exhibits storage stability as well by showing no discernible changes in catalytic efficiency after six months. The leaching of AtPdNP catalyst was studied under three different conditions by suspending 50 mg catalyst in 5 mL distilled water. **A**-Resultant solution was allowed to stir for 24 h, **B**-Solution was sonicated at 80°C for 6 h, **C**-Solution was used for nitro reduction by sodium borohydride for 1 h. Later, the catalyst were separated by filtration and the filtrate solutions were used for the ICP-OES analysis (**Table 01**). Detailed calculations are given in supporting information. The obtained ICP-OES results have clearly demonstrated the negligible leaching of palladium in all the three filtrates (i.e. less than 1.15% ppm). This clearly give the confirmation of heterogeneous nature of prepared catalysis.

Table 01. Catalyst leaching study by ICP-OES

Sample Code	Pd in AtPdNP (PPM)	Pd Leaching (PPM)	Pd Leaching (% PPM)
A	530	3.15	0.59 %
B	530	5.99	1.13 %
C	530	6.03	1.13 %

2.7 Methods of characterization:

UV-Vis spectroscopy was used as primary tool to evaluate catalyst by the absorbance differences between standard Palladium (II) Chloride ($PdCl_2$), standard biomass (At) and the synthesized AtPdNP, covering a 200–800 nm spectral range. All samples were prepared in double-distilled water (DDW). The AtPdNP samples were re-suspended in DDW, homogenized with a homogenizer and sonicated for one hour to ensure proper dispersion. Zeta size and zeta potential for these samples were analysed. Further characterization of lyophilized

powder was carried out using FT-IR spectroscopy, Powder XRD, EDX, XPS. The XPS measurements employed monochromatic Al Kα radiation (1486.6 eV) with an operating power of 50 W (15 kV). The analysed area was set to 300 µm. Survey spectra were recorded with a pass energy of 117.4 eV and an energy step of 0.125 eV, covering a spectral range of 400-2500 eV. For detailed atomic element analysis, a pass energy of 23.5 eV and an energy step of 0.025 eV were applied. The take-off angle was maintained at 25° relative to the sample substrate. To prevent charging during XPS analysis, the samples were neutralized using both low-energy ion and electron beams. SEM, TEM, TGA, and DSC were performed to further characterize the dried AtPdNP, providing insights into their morphology, thermal stability and composition. HPLC was conducted for the monitoring reduction reaction and product characterisation.

3. RESULTS AND DISCUSSION:

3.1. Culture age affects on synthesis of AtPdNP and their catalytic activity:

Aspergillus trinidadensis VM ST01' OL587588 (Fungi) exhibits the following growth behaviors on potato dextrose broth media: a 0–24 h lag phase, a 24–96 h log phase, a 96–120 h stationary phase, and a decline phase after 120 h (**Figure 5**).

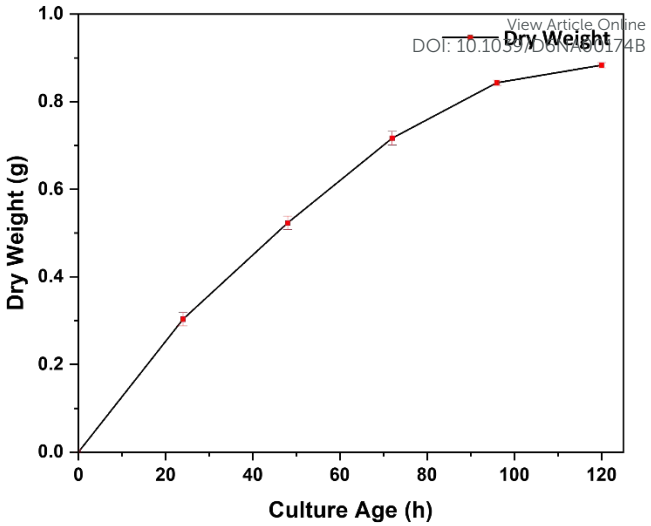

Figure 5: Growth curve of *Aspergillus trinidadensis* VM ST01' OL587588

The best time to use this biomass for the synthesis of palladium nanoparticles was between 24 and 96 h, when the biomass was in the log phase and more enzymes are released by the culture, facilitating the synthesis of nanoparticles. Within this age range, the synthesis of palladium nanoparticles was investigated at 24, 30, 36, 42, 48, and 54 h. According to catalytic activity, AtPdNP prepared with 36 h culture age, converts nitrobenzene to aniline 100% within half hour, making 36 h the ideal culture age (**Table 2**).

Table 2. Nitrobenzene reduction using prepared AtPdNP with varying (At) culture ages

Culture age (h)	Biomass weight (g/mL)	Conversion (%)
24	0.160	94
30	0.160	98
36	0.160	100
42	0.160	98
48	0.160	95
54	0.160	87

The 36 h culture age is the best option for catalytic applications because it exhibits the highest efficiency among all the studied culture ages. All these experiments were performed in triplicate and average results are presented here.

View Article Online
DOI: 10.1039/D6NA00174B

3.2. Effect of biomass quantity on catalytic activity and doping of nanoparticles:

Different biomass amounts with a 36 h culture age were used to optimise biomass quantity for AtPdNP synthesis. Biomass amounts ranging from 0.080 g/mL to 0.240 g/mL were used with a constant palladium concentration of 1 mM. The highest catalytic activity was with biomass concentrations of up to 0.160 g/mL. Beyond this, there was no noticeable increase in catalytic performance, may be due to low palladium uptake with increasing biomass quantity. (**Table 3**) Thus, 0.160 g/mL biomass concentration was used for the remaining optimisation studies. All experiments were performed in triplicate and average results are presented here.

Table 3. Nitrobenzene reduction using prepared AtPdNP with varying biomass quantity

Culture age (hr)	Biomass (g/mL)	Conversion (%)
36	0.080	100
36	0.120	100
36	0.160	100
36	0.200	95
36	0.240	80

3.3 Optimising the incubation period for synthesis of AtPdNP and their catalytic activity:

In this experiment, the optimal culture age of 36 h and biomass amount of 0.160 g/mL was used and the incubation time for the synthesis of palladium nanoparticles were varied to 8, 16 and 24 h. As per the obtained results, best catalytic activity was observed with catalyst prepared by 24 h of incubation (**Table 4**). All these studies were performed in triplicate and average results are presented here.

Table 4. Nitrobenzene reduction using prepared AtPdNP with varying incubation time

Culture age (h)	Biomass (g/mL)	Incubation time (hr)	Conversion (%)
36	0.160	8	30
36	0.160	16	50
36	0.160	24	100

3.4 Controlled experiments for Nitrobenzene reduction

A series of control experiments were conducted to gain a comprehensive understanding of the reaction mechanism and the role of each component. These studies confirmed the critical contribution of each component to the overall reduction process (**Table 5**).

Table 5. Nitrobenzene-NB reduction using prepared AtPdNP (Controlled reaction)

NB mmol	Pd (µmol) AtPdNP	$NaBH_4$ (mmol)	Reaction Time	Conversion in (%)
1	-	-	4 hr	-
1	Blank At	-	4 hr	-
1	Blank At	2	4 hr	-
1	5	-	4 hr	-
1	-	2	4 hr	-
-	5	2	4 hr	-
1	**5**	**2**	**4 hr**	**100 %**

3.5 Kinetic analysis of Nitrobenzene-NB

Due to presence of excess $NaBH_4$ compared with NB, a calculated rate constant of the reaction is a pseudo first-order rate constant (k_{app}). The apparent rate constant was calculated using eqn. (1) for a first-order reaction.[38]

$$\ln [A_t/A_0] = - k_{app}\, t \quad \text{---------- (1)}$$

where A_0 and A_t *are* the absorbance of nitro compounds at initial time and time t in second (s), k_{app} is the apparent rate constant.

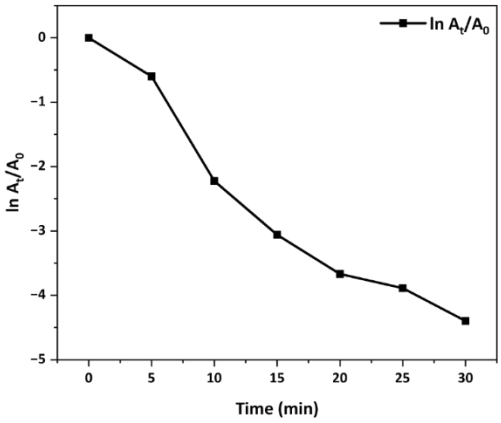

Figure 6: pseudo-first-order for NB to AB

The reaction kinetics was examined by measuring the k_{app} values for the reduction of NB. The rate of reaction was determined by measuring the decrease in the absorption intensity at λ_{max} = 360 nm of the NB with time for the reduction. k_{app} was calculated from the slope obtained by plotting ln(A_t/A_0) *vs.* time (**Figure 6**). All these measurements were performed in triplicate and average results are presented here.

Finally a comparison with palladium nanoparticle as a heterogeneous catalysts, prepared using different techniques and reported in the literature, (**Table S4**) indicates that the present catalyst is a highly efficient and promising alternative.

3.6. Characterization of prepared AtPdNP:

3.6.1 Ultraviolet-Visible Spectroscopy (UV-Vis)

UV-Vis techniques were used to analyse the synthesis of the palladium nanoparticles. Following the synthesis of palladium nanoparticles, the colour of the biomass changes from pale white to brown (**Figure 7b**). In order to prepare the sample, it had to be re-suspended in double-distilled water (DDW), homogenised using a homogeniser, sonicated for an hour, and then taken for UV-Vis examination.

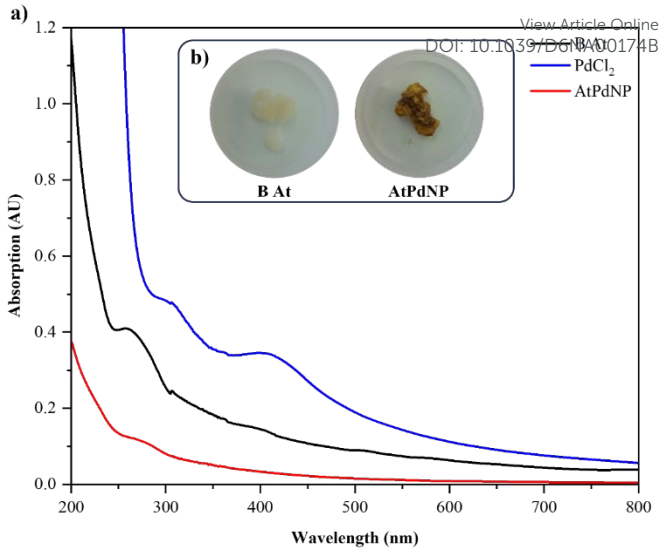

Figure 7: a) UV-Vis spectrum of $PdCl_2$, B At, and AtPdNP, b) Visual analysis of B At and AtPdNP

Because of the protein, blank biomass B-At has an absorbance of 264 nm; on the other hand, blank palladium (II) chloride has an absorbance of 411 nm. The absorbance of palladium (II) chloride vanished following the synthesis of nanoparticles, as observed in the AtPdNP sample. (**Figure 7a**)

3.6.2 Fourier transform infrared spectroscopy

To investigate the chemical composition and functional group involvement in both the native biomass (B At, *Aspergillus trinidadensis* VM ST01) and palladium nanoparticle-incorporated biomass (AtPdNP), FT-IR spectroscopy was employed as a key analytical tool. The spectra provide valuable insights into the interaction between biomolecular functional groups and metal nanoparticles (**Figure 8**). In the case of the blank biomass (B At), the absorption band at 1031 cm^{-1} is attributed to C–N stretching vibrations, which are typically associated with aliphatic amines present in proteins and other nitrogen-containing biomolecules. The presence of multiple bands at 1222, 1373, 1536, and 1640 cm^{-1} further supports the contribution of amide and amine functionalities. Specifically, the band around 1536 cm^{-1} can be assigned to N–H bending (amide

View Article Online
DOI: 10.1039/D6NA00174B

II), while the band near 1640 cm^{-1} corresponds to C=O stretching vibrations of amide I groups,

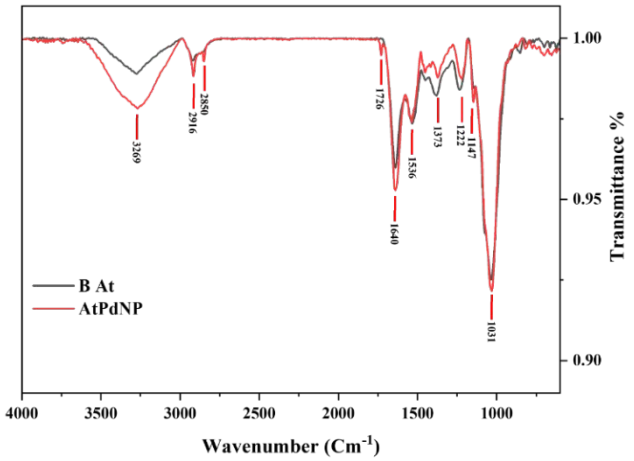

Figure 8: FT-IR spectrum of B-At and AtPdNP

indicating the presence of peptide linkages in fungal proteins. The peaks at 2916 cm^{-1} and 3269 cm^{-1} are attributed to aliphatic C–H stretching and N–H/O–H stretching vibrations, respectively, suggesting the presence of polysaccharides, proteins, and hydroxyl-rich biomolecules within the biomass matrix. Upon doping with palladium nanoparticles (AtPdNP), the FT-IR spectrum retains most of the characteristic bands of the native biomass, confirming that the fundamental biochemical framework remains intact. However, significant changes in peak sharpness, intensity, and slight shifts in wavenumber are observed. These variations indicate strong interactions between palladium nanoparticles and the functional groups of the biomass. Such shifts are commonly associated with coordination or binding of metal nanoparticles with electron-donating groups such as amines, hydroxyls, and carbonyls. Notably, the appearance of new bands at 1147, 1726, and 2850 cm^{-1} in the AtPdNP spectrum provides further evidence of structural modification. The band at 1147 cm^{-1} may be attributed to C–O stretching vibrations, possibly arising from polysaccharide or alcohol groups involved in nanoparticle stabilization. The prominent band at 1726 cm^{-1} corresponds to C=O stretching of carbonyl or ester groups, suggesting oxidation or modification of functional groups during nanoparticle formation. The band at 2850 cm^{-1} is assigned to symmetric C–H stretching of aliphatic chains, indicating alterations in lipid or hydrocarbon environments. These spectral changes strongly suggest that biomolecules present in the fungal biomass—such as proteins, polysaccharides, and other metabolites—play a dual role as reducing as well as stabilizing (capping) agents during the formation of palladium nanoparticles. The interaction between PdNPs and functional groups leads to changes in the vibrational environment, thereby confirming successful incorporation of nanoparticles into the biomass matrix.

Overall, the FT-IR analysis clearly demonstrates that palladium nanoparticle doping induces significant chemical interactions and structural modifications in the biomass, without completely disrupting its inherent biochemical architecture. This supports the hypothesis that the biosynthesized PdNPs are effectively stabilized by the functional groups present in *Aspergillus trinidadensis* biomass, which is crucial for their potential catalytic and environmental applications.

3.6.3 Zeta Size and Zeta Potential

The dynamic light scattering (DLS) analysis revealed that the synthesized Palladium nanoparticles exhibited an average hydrodynamic diameter of 141.8 ± 1.9 nm with a polydispersity index (PDI) of 1.000, indicating moderate size uniformity in the colloidal suspension. The Zeta potential was measured to be −0.472 mV, suggesting a negative surface charge and good colloidal stability due to electrostatic repulsion. These measurements were

View Article Online
DOI: 10.1039/D6NA00174B

carried out at 25 °C in aqueous medium. (**Figure S1, Table S1, Figure S2, and Table S2**)

3.6.4 Thermogravimetric Analysis (TGA) & Differential Scanning Calorimetry (DSC)

Thermal stability, composition, decomposition temperatures, moisture content, melting point, crystallisation point, and thermal events for AtPdNP are examined using thermogravimetric analysis (TGA), differential scanning calorimetry (DSC), and differential thermal analysis (DTA) as shown in **Figure 9**. The initial weight loss for the moisture in Blank At is 7.01% up to 119 °C (**6-a**). After that, the initial sample decomposes from 119 °C to 252 °C, which is 7.23%.

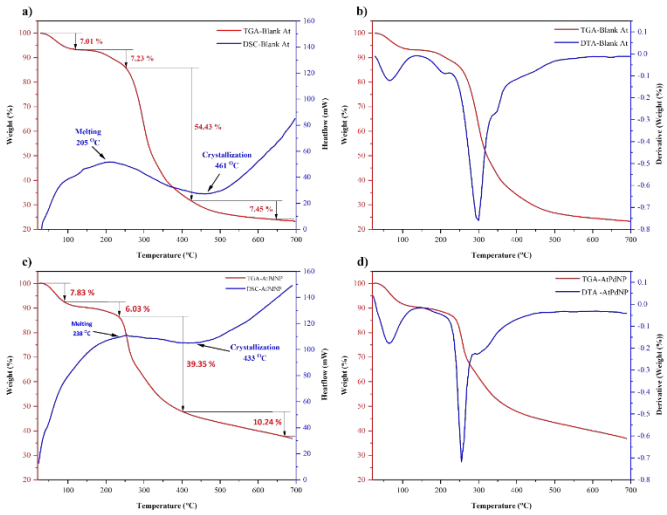

Figure 9: (a) TGA-DSC of Blank At, (b) TGA-DTA of Blank At, (c) TGA-DSC of AtPdNP, and (d) TGA-DTA of AtPdNP

The sample's major decomposition occurs at a faster rate up to 425 °C, 54.43%, and the final decomposition is slower up to 647 °C, which is 7.25%. The total decomposition of the sample is 75.92%, leaving carbon ash at the end. Biomass is melting at 205 °C temperature and goes to crystallization at 461 °C temperature. The thermal analysis of Blank At reveals two distinct thermal events **(6-b)**. The first event, associated with the initial decomposition of moisture, exhibits a broad and shallow peak at 65 °C. The second major thermal event occurs at 297 °C, where the sample undergoes significant decomposition. The initial weight loss for the moisture in AtPdNP is 7.83% up to 91 °C (**6-c**). After that, the initial sample decomposes from 91 °C to 234 °C, which is 6.03%. The sample's major decomposition occurs at a faster rate up to 400 °C, 39.35%, and the final decomposition is slower up to 670 °C, which is 10.24%. Total decomposition of the sample is 63.45%, leaving carbon ash and Palladium oxide at the end. The AtPdNP melting at 238 °C temperature and goes to crystallization at 433 °C temperature. The thermal analysis of AtPdNP also reveals two distinct thermal events (**6-d**). The first event, associated with the initial decomposition of moisture, exhibits a broad and shallow peak at 62 °C. The second major thermal event occurs at 255 °C, where the sample undergoes significant decomposition.

3.6.5 X-ray photoelectron spectroscopy (XPS)

XPS measurements was performed to determine the composition present in blank sample of *Aspergillus trinidadensis* VM ST01 biomass (B-At) and biomass doped with PdNP (AtPdNP). A binding energy for carbon 1s at 284.8 eV, nitrogen 1s at 399.8 eV, and oxygen 1s at 532.8 eV were presented in the B-At. However in case of AtPdNP, two more binding energy at 336.80 eV and 342.80 eV from Pd0 correspond to the Pd3d5/2 and Pd3d3/2, respectively were present (**Figure 10**).[17] These energies are relatively high for Pd0, which may be due to the interaction between Pd NPs and oxygen/nitrogen contained groups within lignin during the carbonization process.[18] Also it is noted that the Pd3d spectrum of Pd-0.3 sample showed no peaks corresponding to Pd^{2+} at 338.00 eV and 343.30 eV, respectively and indicated absence of Pd^{2+} species. These results confirmed the

successful reduction and nucleation of Pd NPs in one-pot synthesis.

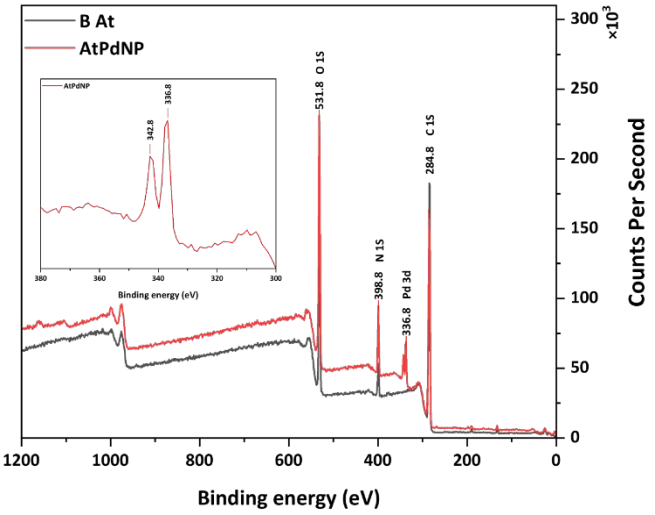

Figure 10: XPS spectroscopy of B-At and AtPdNP

3.6.6 Powder X-ray Powder Diffraction

Powder XRD was used to analyse the crystalline nature of AtPdNP catalyst. Since palladium was not doped into the culture, Blank At biomass was used as a reference (**Fig. 11a**). AtPdNP prepared with 1mM (**Fig. 11b**) Palladium chloride was used for Powder XRD analysis. A small but very sharp hump-shaped peak was observed between 30 and 40 degrees, guaranteeing the deviates from Blank At, although it is not very noticeable. As a result, AtPdNP sample was prepared with double concentration of 2mM Palladium chloride (**Fig. 11c**). Increasing amounts of palladium was clearly observed between 30 and 40 degrees, a noticeable hump-shaped peak has seen in the sample analysis.

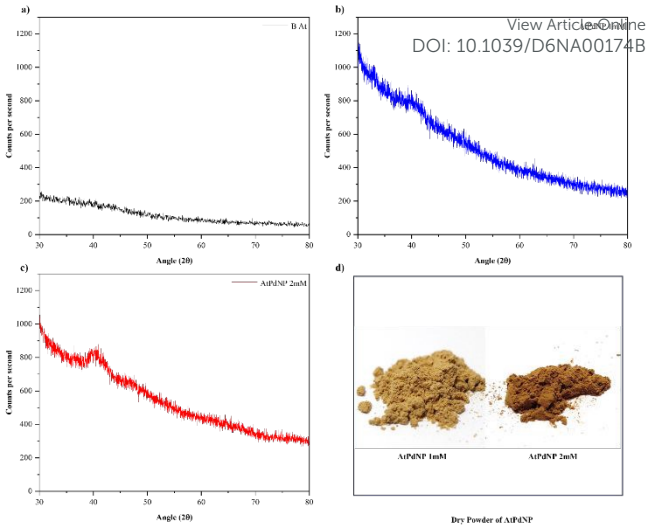

Figure 11: (**a**) Powder XRD of Blank At, (**b**) Powder XRD of AtPdNP 1mM, (**c**) Powder XRD of AtPdNP 2mM, (**d**) Visual difference between AtPdNP 1mM and AtPdNP 2mM

The noticeable colour difference between the catalyst made from 1 mM and 2 mM palladium solution was also observed (**Fig. 8d**).

3.6.7 Scanning Electron Microscope (SEM)

Scanning electron microscope (SEM) study was performed to analyse the surface morphology of catalyst AtPdNP (**Figure 12**). As palladium was not doped into the culture, Blank At was used as a reference (**a**). This sample was not having any dots in SEM images, confirming the absence of PdNPs. However, on the other hand, the SEM image of catalyst AtPdNP, where palladium was doped in the culture, numbers of small dots were easily visible, confirming the doping of palladium nanoparticles.

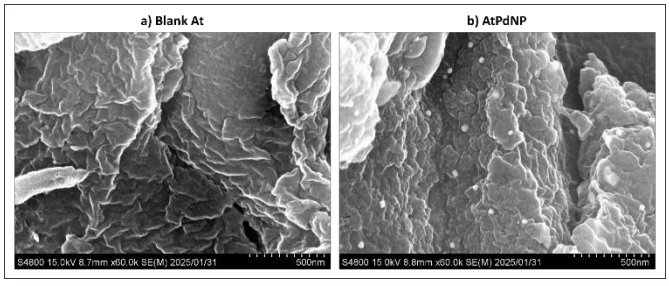

Figure 12: SEM images of (**a**) Blank At and (**b**) catalyst AtPdNP

View Article Online
DOI: 10.1039/D6NA00174B

Also due to presence of palladium, the surface of AtPdNP was much smooth compare to blank biomass.

3.6.8 Transmission Electron Microscope (TEM)

TEM analysis was used to study the bulk morphology and size distribution of palladium nanoparticles (AtPdNP) produced by *Aspergillus trinidadensis*. The TEM images have demonstrated that the palladium nanoparticles were successfully doped and stabilised by biomass of *Aspergillus trinidadensis* (**Figure 13**).

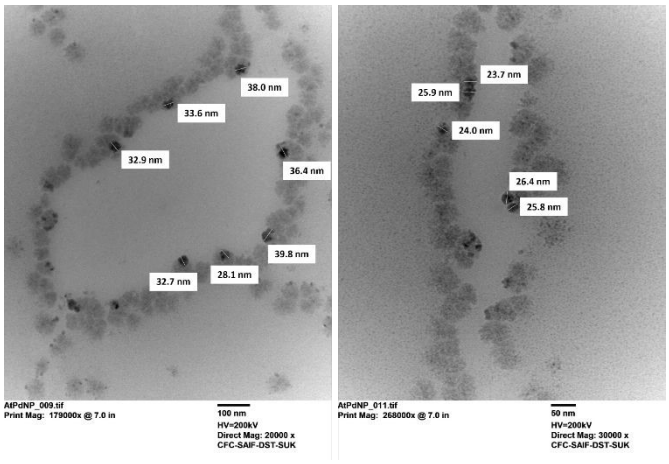

Figure 13: TEM Image of AtPdNP

The TEM SEAD pattern indicated that the sample was amorphous overall, which may due to the extremely low concentration of palladium nanoparticles (atomic percentage of 0.01%), which was also validated by TEM-EDX. While metals exhibit a crystalline nature, their amorphous form was due to extremely low palladium concentration and relatively very high concentration of cell components. The examination on nano scale has shown that the palladium nanoparticles became apparent in the size range from 20 to 40 nm. The TEM analysis has clearly demonstrated the successful doping of palladium nano particles by biological moieties of *Aspergillus trinidadensis*. The particle size distribution graph (**Figure 14**) displayed a Gaussian shape, and the average particle diameter was 30.33 ± 3.56 nm.

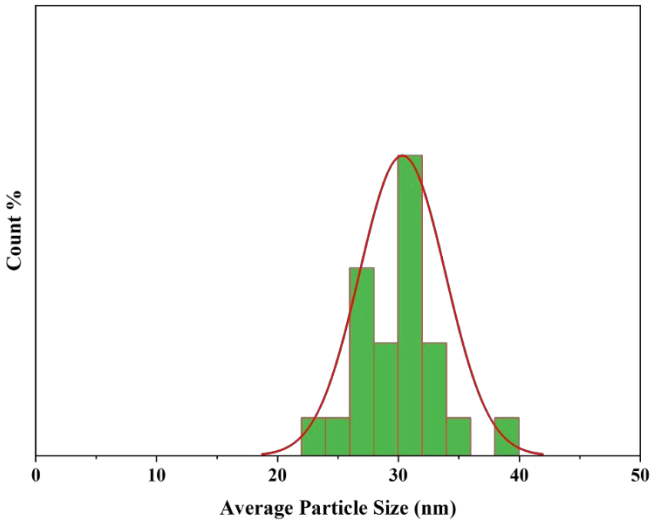

Figure 14: Size distribution curve of AtPdNP

The observed size range was between 20 nm - 40 nm, indicating a relatively limited size distribution suitable for catalytic applications.

3.6.9 Energy Dispersive X-ray (EDX) and Colour Mapping

Energy Dispersive X-ray Spectroscopy (EDX) was employed to analyse the elemental composition of the synthesized palladium nanoparticle as heterogeneous catalyst. As shown in the EDX spectrum without grid (**Figure 15**), characteristic signals for palladium (Pd) were detected, along with peaks for carbon (C), nitrogen (N), and oxygen (O). These additional elements were certainly originate from the biological components or natural capping agents introduced during the green synthesis process.

According to the elemental analysis data (**Table 6**), palladium was present at an atomic percentage of 0.01%, confirming its successful incorporation into the nanostructure.

View Article Online
DOI: 10.1039/D6NA00174B

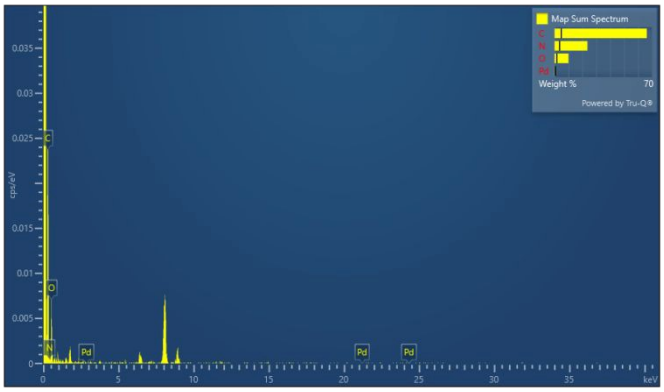

Figure 15: EDX Spectrum of AtPdNP

Table 6. EDX Map Sum Spectrum of AtPdNP

Sr. No.	Element	Line Type	k Factor	Absorption Correction	Wt %	Wt % Sigma	Atomic %
1	C	K series	2.787	1.00	66.31	4.76	70.50
2	N	K series	3.538	1.00	23.58	3.61	21.50
3	O	K series	2.033	1.00	10.01	1.61	7.99
4	Pd	K series	8.754	1.00	0.10	0.62	0.01
	Total				100.00		100.00

The dominant presence of carbon (70.50%), nitrogen (21.50%) and oxygen (7.99%) points to the involvement of biomolecules derived from the fungal extract used as a reducing and stabilizing agent. The colour mapping of AtPdNP were also displayed (**Figure 16**), where colour dots represented carbon, nitrogen and oxygen.

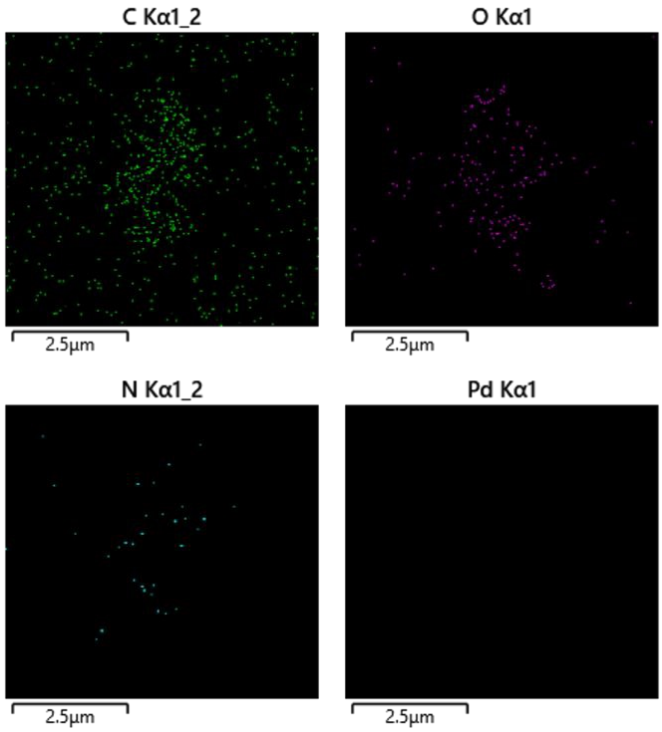

Figure 16: EDX colour mapping of AtPdNP

3.6.10 HPLC (High-Performance Liquid Chromatography)

View Article Online
DOI: 10.1039/D6NA00174B

Palladium element was not displaying much because of its extremely low concentration. Overall, the EDX results have supported the effective biosynthesis of the Pd nanoparticles and offered insight into the surface chemistry influenced by the green synthesis method. The conversion of nitrobenzene to aniline was monitored by HPLC. The HPLC chromatogram of the synthesized Aniline displayed a single, sharp peak at a retention time (Rt) of 7.886 minutes, which has matched with the retention time of the authentic reference standard Aniline. This has confirmed the successful formation of the target product. In contrast, nitrobenzene starting material exhibited a major peak at (Rt) 10.827 minutes, indicating that the product was chemically distinct from the precursor. The purity of the synthesized Aniline, based on peak area, was found to be 96.74%, signifying minimal presence of impurities. This chromatographic analysis was carried out on a C18 reverse-phase column (4.6 × 250 mm, 5 µm) using a mobile phase of acetonitrile and water (70:30, v/v) under isocratic conditions at a flow rate of 0.5 mL/min and detection wavelength of 254 nm. The consistency in retention time with the standard and the absence of the starting compound peak confirmed the complete conversion and high purity of the final product (**Figure S3 and Table S3**).

4. Conclusion:

Here we have demonstrated *Aspergillus trinidadensis* as an efficient microbe for the biosynthesis of AtPdNP. A one-pot method that is sustainable, eco-friendly and efficient has been established. UV-Vis, FT-IR, TGA-DSC-DTA, XPS, SEM, TEM, EDX, Elemental Mapping, Powder XRD and Zita potential analysis were all used to fully characterize the morphologies of AtPdNP. All these analysis has confirmed the formation of palladium nano particle with uniform size distribution from 20 to 40 nm. Also it has confirmed the efficient capping of palladium nano particles by biomass. Nitrobenzene reduction has been used to demonstrate the use of the produced catalyst. As a catalytic investigation, AtPdNP produced under various circumstances was employed. The highest reduction efficiency was demonstrated by AtPdNP synthesized through 160 g/mL biomass of 36-hour culture age under 24-hour incubation at 34 °C.

Acknowledgment

The authors would like to acknowledge the financial support from GSBTM and SHODH Scheme, Govt. of Gujarat (Ref No: 202301733). We acknowledge SAIF, Shivaji University, Kolhapur, for TEM-EDX analysis, SAIF, Panjab University, Chandigarh, for Powder-XRD analysis, CHARUSAT, Changa, for TGA-DSC analysis, and Miyazaki University, Japan, for XPS and SEM analysis. Authors are also thankful to Aether Industry Ltd. for LC-MS analysis.

Author Contributions

All the experiments were designed and performed by Hemal B. Rathod and Paresh N. Patel. The spectral study, interpretation, and correlations were done by Hemal B. Rathod, Amar G. Deshmukh, Yashasvi N. Desai and Paresh N. Patel. The manuscript was written by Hemal B. Rathod. The final proofreading and editing were done by Paresh N. Patel.

Conflict of Interest

The authors declare that they have no known competing financial interests or personal relationships that could have appeared to influence the work reported in this paper.

Supplementary materials

Supplementary material associated with this article can be found, in the online version, at…

View Article Online
DOI: 10.1039/D6NA00174B

Reference

1. Gulbagca F, Aygün A, Gülcan M, Ozdemir S, Gonca S, Şen F. Green synthesis of palladium nanoparticles: Preparation, characterization, and investigation of antioxidant, antimicrobial, anticancer, and DNA cleavage activities. Appl Organomet Chem. 2021;35(8):e6272.
2. Sharaby MR, Soliman EA, Abdel-Rahman AB, Osman A, Khalil R. Novel pectin-based nanocomposite film for active food packaging applications. Sci Rep. 2022;12(1):20673.
3. Bachmann G, Holtmannspötter D, Korte S, Zweck A. Angels on a pinhead: new research networks for nanotechnology. Foresight. 2001;3(4):331–9.
4. West JL, Halas NJ. Applications of nanotechnology to biotechnology: Commentary. Curr Opin Biotechnol. 2000;11(2):215–7.
5. Thiruvengadam M, Rajakumar G, Chung IM. Nanotechnology: current uses and future applications in the food industry. 3 Biotech. 2018;8:1–13.
6. Thakkar KN, Mhatre SS, Parikh RY. Biological synthesis of metallic nanoparticles. Nanomedicine nanotechnology, Biol Med. 2010;6(2):257–62.
7. Sepeur S. Nanotechnology: technical basics and applications. Vincentz Network GmbH & Co KG; 2008.
8. Şahin B, Aygün A, Gündüz H, Şahin K, Demir E, Akocak S, et al. Cytotoxic effects of platinum nanoparticles obtained from pomegranate extract by the green synthesis method on the MCF-7 cell line. Colloids Surfaces B Biointerfaces. 2018;163:119–24.
9. Parsons JG, Peralta-Videa JR, Gardea-Torresdey JL. Use of plants in biotechnology: synthesis of metal nanoparticles by inactivated plant tissues, plant extracts, and living plants. Dev Environ Sci. 2007;5:463–85.
10. Singaravelu G, Arockiamary JS, Kumar VG, Govindaraju K. A novel extracellular synthesis of monodisperse gold nanoparticles using marine alga, Sargassum wightii Greville. Colloids surfaces B Biointerfaces. 2007;57(1):97–101.
11. Luangpipat T, Beattie IR, Chisti Y, Haverkamp RG. Gold nanoparticles produced in a microalga. J Nanoparticle Res. 2011;13:6439–45.
12. Makarov V V, Love AJ, Sinitsyna O V, Makarova SS, Yaminsky I V, Taliansky ME, et al. "Green" nanotechnologies: synthesis of metal nanoparticles using plants. Acta Naturae (англоязычная версия). 2014;6(1 (20)):35–44.
13. Mittal AK, Chisti Y, Banerjee UC. Synthesis of metallic nanoparticles using plant extracts. Biotechnol Adv. 2013;31(2):346–56.
14. Dahl JA, Maddux BLS, Hutchison JE. Toward greener nanosynthesis. Chem Rev. 2007;107(6):2228–69.
15. Al-Shmgani HSA, Mohammed WH, Sulaiman GM, Saadoon AH. Biosynthesis of silver nanoparticles from Catharanthus roseus leaf extract and assessing their antioxidant, antimicrobial, and wound-healing activities. Artif cells, nanomedicine, Biotechnol. 2017;45(6):1234–40.
16. Sulaiman GM, Tawfeeq AT, Jaaffer MD. Biogenic synthesis of copper oxide nanoparticles using olea europaea leaf extract and evaluation of their toxicity activities: An in vivo and in vitro study. Biotechnol Prog. 2018;34(1):218–30.
17. Sulaiman GM, Tawfeeq AT, Naji AS. Biosynthesis, characterization of magnetic iron oxide nanoparticles and evaluations of the cytotoxicity and DNA damage of human breast carcinoma cell lines. Artif cells, nanomedicine, Biotechnol. 2018;46(6):1215–29.

View Article Online
DOI: 10.1039/D6NA00174B

18. Taha ZK, Hawar SN, Sulaiman GM. Extracellular biosynthesis of silver nanoparticles from Penicillium italicum and its antioxidant, antimicrobial and cytotoxicity activities. Biotechnol Lett. 2019;41:899–914.
19. Hamelian M, Zangeneh MM, Amisama A, Varmira K, Veisi H. Green synthesis of silver nanoparticles using Thymus kotschyanus extract and evaluation of their antioxidant, antibacterial and cytotoxic effects. Appl Organomet Chem. 2018;32(9):e4458.
20. Ahmeda A, Zangeneh A, Zangeneh MM. Preparation, formulation, and chemical characterization of silver nanoparticles using Melissa officinalis leaf aqueous extract for the treatment of acute myeloid leukemia in vitro and in vivo conditions. Appl Organomet Chem. 2020;34(2):e5378.
21. Mohammadi G, Zangeneh MM, Zangeneh A, Haghighi ZMS. Chemical characterization and anti-breast cancer effects of silver nanoparticles using Phoenix dactylifera seed ethanolic extract on 7, 12-Dimethylbenz [a] anthracene-induced mammary gland carcinogenesis in Sprague Dawley male rats. Appl Organomet Chem. 2020;34(1):e5136.
22. Zangeneh MM, Ghaneialvar H, Akbaribazm M, Ghanimatdan M, Abbasi N, Goorani S, et al. Novel synthesis of Falcaria vulgaris leaf extract conjugated copper nanoparticles with potent cytotoxicity, antioxidant, antifungal, antibacterial, and cutaneous wound healing activities under in vitro and in vivo condition. J Photochem Photobiol B Biol. 2019;197:111556.
23. Zangeneh MM, Bovandi S, Gharehyakheh S, Zangeneh A, Irani P. Green synthesis and chemical characterization of silver nanoparticles obtained using Allium saralicum aqueous extract and survey of in vitro antioxidant, cytotoxic, antibacterial and antifungal properties. Appl Organomet Chem. 2019;33(7):e4961.
24. Zangeneh MM, Joshani Z, Zangeneh A, Miri E. Green synthesis of silver nanoparticles using aqueous extract of Stachys lavandulifolia flower, and their cytotoxicity, antioxidant, antibacterial and cutaneous wound-healing properties. Appl Organomet Chem. 2019;33(9):e5016.
25. Seydi N, Mahdavi B, Paydarfard S, Zangeneh A, Zangeneh MM, Najafi F, et al. Preparation, characterization, and assessment of cytotoxicity, antioxidant, antibacterial, antifungal, and cutaneous wound healing properties of titanium nanoparticles using aqueous extract of Ziziphora clinopodioides Lam leaves. Appl Organomet Chem. 2019;33(9):e5009.
26. Mahdavi B, Saneei S, Qorbani M, Zhaleh M, Zangeneh A, Zangeneh MM, et al. Ziziphora clinopodioides Lam leaves aqueous extract mediated synthesis of zinc nanoparticles and their antibacterial, antifungal, cytotoxicity, antioxidant, and cutaneous wound healing properties under in vitro and in vivo conditions. Appl Organomet Chem. 2019;33(11):e5164.
27. Deshmukh AG, Mistry V, Sharma A, Patel PN. Green and sustainable bio-synthesis of gold nanoparticles using Aspergillus Trinidadensis VM ST01: Heterogeneous catalyst for nitro reduction in water. Tetrahedron Green Chem [Internet]. 2023;2:100021. Available from: https://doi.org/10.1016/j.tgchem.2023.100021
28. Bendre AD, Patil VP, Terdale SS, Kodam KM, Waghmode SB. A simple, efficient and green approach for the synthesis of palladium nanoparticles using Oxytocin: Application for ligand free Suzuki reaction and total synthesis of aspongpyrazine A. J Organomet Chem. 2020;909:121093.

29. Veerakumar P, Lin KC. An overview of palladium supported on carbon-based materials: Synthesis, characterization, and its catalytic activity for reduction of hexavalent chromium. Chemosphere. 2020;253:126750.
30. Kora AJ, Rastogi L. Green synthesis of palladium nanoparticles using gum ghatti (Anogeissus latifolia) and its application as an antioxidant and catalyst. Arab J Chem. 2018;11(7):1097–106.
31. Nasrollahzadeh M, Maham M, Tohidi MM. Green synthesis of water-dispersable palladium nanoparticles and their catalytic application in the ligand-and copper-free Sonogashira coupling reaction under aerobic conditions. J Mol Catal A Chem. 2014;391:83–7.
32. Qazi F, Hussain Z, Tahir MN. Advances in biogenic synthesis of palladium nanoparticles. RSC Adv. 2016;6(65):60277–86.
33. Gioria E, Signorini C, Wisniewski F, Gutierrez L. Green synthesis of time-stable palladium nanoparticles using microfluidic devices. J Environ Chem Eng. 2020;8(5):104096.
34. Nagaraja K, Prasad B, Almarhoon ZM, Oh TH. Green multifunctional palladium nanoparticles from polysaccharide cordia myxa (CMY) gum: Synthesis, characterization, and antibacterial activity. Colloids Surfaces A Physicochem Eng Asp. 2023;679:132612.
35. Pechyen C, Tangnorawich B, Toommee S, Marks R, Parcharoen Y. Green Synthesis of Metal Nanoparticles, Characterization, and Biosensing Applications. Sensors Int. 2024;100287.
36. Baran NY, Baran T, Nasrollahzadeh M. Synthesis of palladium nanoparticles stabilized on Schiff base-modified ZnO particles as a nanoscale catalyst for the phosphine-free Heck coupling reaction and 4-nitrophenol reduction. Sci Rep. 2023;13(1):12008.
37. Deshmukh AG, Rathod HB, Patel PN. Fungus reinforced sustainable gold nanoparticles: An efficient heterogeneous catalyst for reduction of nitro aliphatic, aromatic and heterocyclic scaffolds. Results Chem. 2023;6:101199.
38. Trzeciak AM, Augustyniak AW. The role of palladium nanoparticles in catalytic C–C cross-coupling reactions. Coord Chem Rev. 2019; 384: 1–20.
39. Veisi H, Rashtiani A, Barjasteh V. Biosynthesis of palladium nanoparticles using Rosa canina fruit extract and their use as a heterogeneous and recyclable catalyst for Suzuki–Miyaura coupling reactions in water. Appl Organomet Chem. 2016; 30(4): 231–5.
40. Favier I, Pla D, Gómez M. Palladium nanoparticles in polyols: Synthesis, catalytic couplings, and hydrogenations. Chem Rev. 2019;120(2):1146–83.
41. Alkhalidi HM, Zaman U, Khan D, ur Rehman K, Omar KI, Alissa M, et al. Microwave assisted eco-benign synthesis of novel palladium nanoparticles (ACPs-PdNPs): A new insight into photocatalytic and biomedical applications. J Mol Liq. 2023;392:123469.
42. Yen CH, Wei H, Lin H, Tan C. Synthesis and application of palladium stearates as precursors for the preparation of palladium nanoparticles. Appl Organomet Chem. 2012;26(12):736–42.
43. Parveen K, Banse V, Ledwani L. Green synthesis of nanoparticles: Their advantages and disadvantages. In: AIP conference proceedings. AIP Publishing; 2016.
44. Jamkhande PG, Ghule NW, Bamer AH, Kalaskar MG. Metal nanoparticles synthesis: An overview on methods of preparation, advantages and disadvantages, and applications. J Drug Deliv Sci Technol. 2019;53:101174.
45. Ramanathan S, Gopinath SCB, Arshad MKM, Poopalan P, Perumal V. Nanoparticle synthetic

methods: strength and limitations. In: Nanoparticles in Analytical and Medical Devices. Elsevier; 2021. p. 31–43.

46. Mohana S, Sumathi S. Multi-functional biological effects of palladium nanoparticles synthesized using Agaricus bisporus. J Clust Sci. 2020; 31: 391–400.

47. Veisi H, Tamoradi T, Karmakar B, Mohammadi P, Hemmati S. In situ biogenic synthesis of Pd nanoparticles over reduced graphene oxide by using a plant extract (Thymbra spicata) and its catalytic evaluation towards cyanation of aryl halides. Mater Sci Eng C. 2019; 104: 109919.

View Article Online
DOI: 10.1039/D6NA00174B

View Article Online
DOI: 10.1039/D6NA00174B

Data Availability Statement

Additional data related to main manuscript are available in supporting information.